Biochemical Journal (2023) **480** 1183–1197
https://doi.org/10.1042/BCJ20230129

PORTLAND PRESS

Research Article

Photoaffinity labelling displacement assay using multiple recombinant protein domains

David J. Fallon[1,2], Alex Phillipou[3], Christopher J. Schofield[4], David House[1], Nicholas C. O. Tomkinson[2] and Jacob T. Bush[1]

[1]Department of Chemical Biology, GSK R&D, Gunnels Wood Road, Stevenage SG1 2NY, U.K.; [2]Department of Pure and Applied Chemistry, University of Strathclyde, Thomas Graham Building, Glasgow G1 1XL, U.K.; [3]Department of Screening, Profiling and Mechanistic Biology, GSK R&D, Gunnels Wood Road, Stevenage SG1 2NY, U.K.; [4]Chemistry Research Laboratory, Department of Chemistry and the Ineos Oxford Institute for Antimicrobial Research, University of Oxford, 12 Mansfield Road, Oxford OX1 3TA, U.K.

Correspondence: Jacob T. Bush (jacob.x.bush@gsk.com) or Nicholas C. O. Tomkinson (nicholas.tomkinson@strath.co.uk)

The development and optimisation of a photoaffinity labelling (PAL) displacement assay is presented, where a highly efficient PAL probe was used to report on the relative binding affinities of compounds to specific binding sites in multiple recombinant protein domains in tandem. The N- and C-terminal bromodomains of BRD4 were used as example target proteins. A test set of 264 compounds annotated with activity against the bromodomain and extra-terminal domain (BET) family in ChEMBL were used to benchmark the assay. The pIC_{50} values obtained from the assay correlated well with orthogonal TR-FRET data, highlighting the potential of this highly accessible PAL biochemical screening platform.

Introduction

Advances in genomics and recombinant protein technology over the last three decades has spurred target-based drug discovery to become the dominant method for finding new small molecule therapeutics [1,2]. Recombinant protein technologies allow for targets to be expressed and purified for use in biochemical or biophysical screening assays to identify small molecule ligands [3,4]. The automation and miniaturisation of assay formats have also aided the development of high throughput platforms, which are used for both hit identification and lead optimisation [5]. Due to the speed of analysis, sensitivity, dynamic range and the ability to miniaturise, the majority of assays for lead optimisation cycles are fluorescence-based [6]. These include time-resolved fluorescence resonance energy transfer (TR-FRET), AlphaScreen™, and fluorescence polarisation (FP) assays [7–9]. One caveat to these fluorescence-based biochemical assay platforms is that only one recombinant protein can be screened per experiment. For each new target protein of interest, a new assay needs to be developed and optimised. A biochemical method capable of screening multiple proteins simultaneously would enable the optimisation of potencies (and hence selectivities) against both on- and off-targets in a single assay. Such a method would be useful at the lead optimisation stage of small molecule drug discovery, as more information-rich assays may help to reduce candidate cycle times [10].

Photoaffinity labelling (PAL) probes are used to report on non-covalent interactions formed by their parent affinity function; the component of the PAL probe designed for binding to target proteins [11]. PAL probes are typically incubated with a biological mixture (recombinant protein, cell lysate, or live cells) and irradiated with UV light. This irradiation leads to a short-lived reactive intermediate, which can covalently label neighbouring protein residues and inform on the non-covalent interactions prior to irradiation. Subsequent analysis by intact protein LCMS provides an information-rich readout, where labelling stoichiometry and the mass of the labelling species can be determined accurately (Figure 1A). This readout allows for multiple proteins to be analysed within the same assay, providing a unique advantage over fluorescence-based biochemical screening methods that can only be used to study the binding of ligands to a single protein.

Received: 12 April 2023
Revised: 15 June 2023
Accepted: 3 July 2023

Accepted Manuscript online: 4 July 2023
Version of Record published: 31 August 2023

Biochemical Journal (2023) 480 1183–1197
https://doi.org/10.1042/BCJ20230129

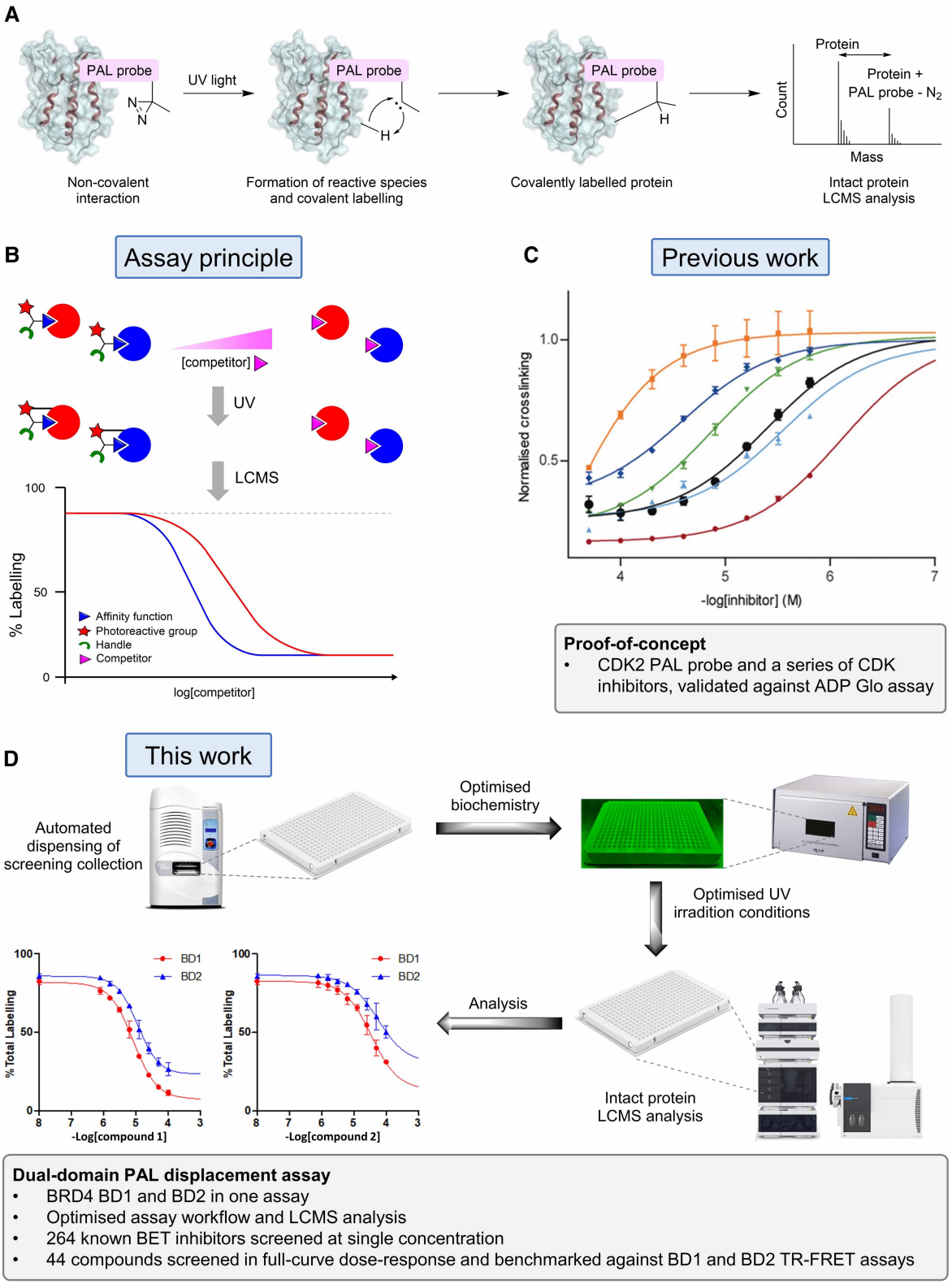

Figure 1. Principle behind the photoaffinity displacement assay proposed in this work. Part 1 of 2

(**A**) PAL workflow with recombinant protein, using a diazirine-based PAL probe as an example. (**B**) Principle behind PAL displacement assay. A concentration gradient of competitor compound is incubated with a fixed concentration of PAL probe. Upon irradiation, the PAL probe labels the protein domain, and any percentage labelling is proportional to the amount of PAL

Biochemical Journal (2023) **480** 1183–1197
https://doi.org/10.1042/BCJ20230129

Figure 1. Principle behind the photoaffinity displacement assay proposed in this work. Part 2 of 2
probe non-covalently bound to the target protein at equilibrium. (**C**) Previous work, carried out by Grant et al. where a series of CDK inhibitors were used to validate the PAL displacement assay. Each curve represents a normalised displacement assay of a different CDK inhibitor against CDK2. (**D**) This work, involving the optimisation of the PAL assay platform using two recombinant protein domains. Two hundred and sixty-four known BET inhibitors were used to benchmark the platform against the BD1 and BD2 domains of BRD4.

A PAL probe can be displaced from a protein binding site by a competitive ligand prior to irradiation, and the affinity of the competitive ligand can be determined by screening a range of ligand concentrations against a fixed concentration of PAL probe (Figure 1B) [11–14]. The Cheng–Prusoff equation can then be used to derive an apparent K_d value for the competitive ligand [15]. Grant et al. [16] demonstrated a proof-of-concept for this type of PAL displacement assay, using a pan-CDK PAL probe to measure relative potencies of a series of known CDK inhibitors (Figure 1C). This method showed a good correlation with an orthogonal CDK2 ADP-Glo assay, highlighting the potential for this PAL displacement assay to be developed further.

Recent studies have shown that selective inhibition of the BD1 or BD2 domains of the BET family of proteins produces different phenotypic effects, with BD2 selective inhibitors showing greater efficacy in inflammatory and autoimmune disease models [17,18]. Efforts towards developing selective BD1 and BD2 inhibitors have relied on independent biochemical assays for each domain to determine selectivity. For example, Law et al. [19] used two different TR-FRET assays to develop the BD2 selective inhibitor GSK340. To develop the BD2 selective inhibitor ABBV-744, Faivre et al. [20] used a variety of techniques to determine BRD4 BD1/BD2 selectivity, including TR-FRET, surface plasmon resonance (SPR), and NanoBRET on each individual bromodomain.

Within this report, we describe the development of a dual-domain PAL displacement assay, using recombinant BRD4 N-terminal (BD1) and C-terminal (BD2) domains as target proteins (Figure 1D). A diverse collection of known bromodomain extra-terminal (BET) inhibitors were used to validate the assay and performance was benchmarked against TR-FRET BRD4 BD1 and BD2 assay data.

Results

Choosing an appropriate PAL displacement probe

To identify an optimal PAL probe for the assay, crosslinking yields were determined for 15 BET PAL probes (**1**–**15**) to BD1 and BD2. The probes contained five different photoreactive moieties and three linker lengths, features which can have a significant influence on photocrosslinking yield (Figure 2A,B) [14]. Tetrafluoroaryl azide probe **1** (Figure 2C) gave the highest average levels of photolabelling to BD1 and BD2 (*ca.* 90% total labelling by intact protein LCMS). This probe also showed fast rates of photolabelling to BD1 and BD2, reaching full photoactivation within one minute of irradiation at 302 nm (Figure 2D).

An advantage of determining photocrosslinking yields by intact protein LCMS is the ability to determine the stoichiometry of labelling events, which can be more challenging using fluorescent-based approaches and lead to erroneous results [21]. Probe **1** showed single and double labelling events to both BD1 and BD2 (Figure 2E). To determine how much could be attributed to specific labelling, a displacement experiment was performed with a high concentration of a non-photoreactive analogue of the affinity function, **16** (200 μM, 20-fold excess). In the presence of competitor, the crosslinking yield was reduced to 14%, which can be attributed to non-specific labelling (Supplementary Figure S1).

Active protein concentration

To determine the lower limit for a PAL displacement assay, it was necessary to determine the active concentration of protein [22]. For this experiment, BD1 (*ca.* 1 μM as determined by NanoDrop) and BD2 (*ca.* 2 μM) were irradiated with probe **1** over a range of concentrations (0.2–6.0 μM), which were expected to be in the tight-binding range for the probe (TR-FRET values for probe **1** at BD1 and BD2 were $pIC_{50} = 7.8$ and 7.3, respectively, Figure 3A) [14]. The resulting crosslinking yield followed a linear relationship, owing to the increasing occupancy of the BRD binding site. After the point at which the concentration of **1** was equal to the concentration of active protein, any additional slope would be due to non-specific binding. The point at which

Biochemical Journal (2023) **480** 1183–1197
https://doi.org/10.1042/BCJ20230129

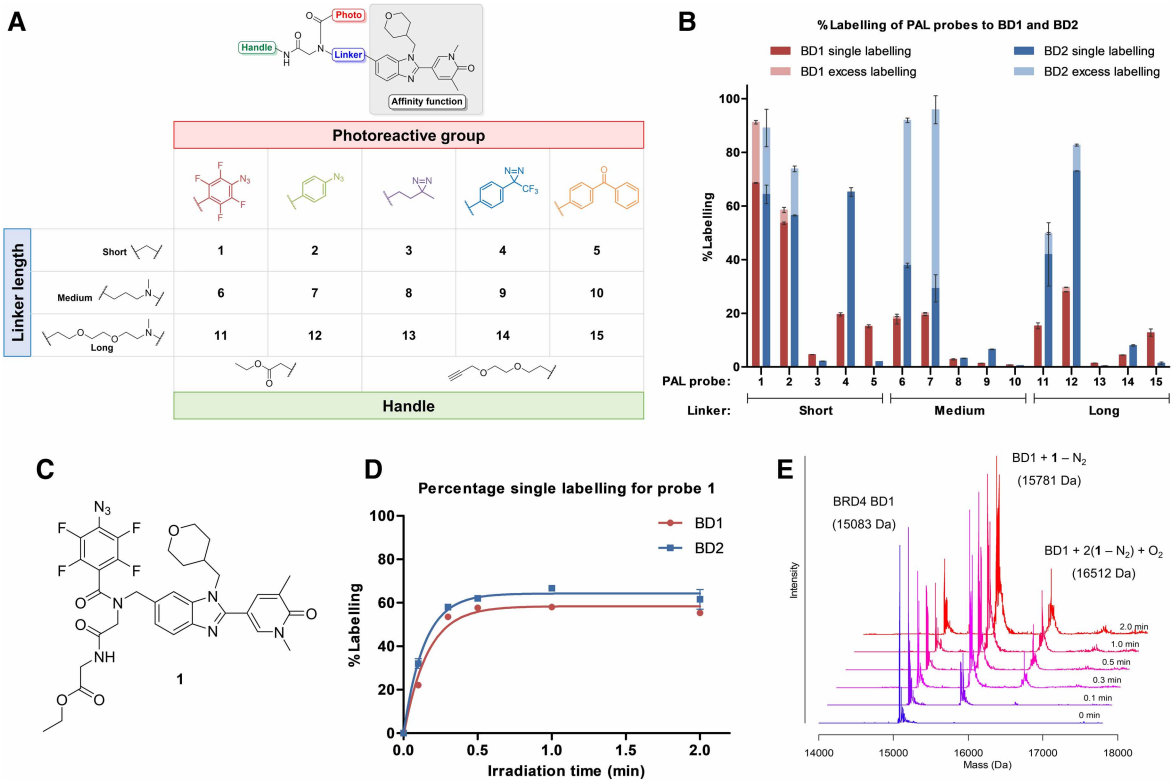

Figure 2. Choosing an optimal PAL probe.

(**A**) Structures of the 15 PAL probes examined to identify an optimal displacement PAL probe. (**B**) Photocrosslinking yields of probes **1**–**15** (5 μM) to BRD4 BD1 and BD2 (1 μM each) after irradiation (302 nm, 10 min) determined by intact protein LCMS. (**C**) Probe **1** was identified as the optimal probe with the highest levels of single labelling to both BD1 and BD2. (**D**) Rates of photolabelling of BD1 and BD2 by probe **1**. (**E**) Detailed photocrosslinking time course for probe **1**. The deconvoluted spectra show the unlabelled protein (15 083 Da), protein with one labelling event (15 781 Da), and protein with two labelling events with the addition of O_2 (16 512 Da) by probe **1**.

the two slopes intersected, the active concentration of protein, was 1.2 μM and 1.3 μM for BD1 and BD2, respectively. Subsequently, LCMS analysis of a range of concentrations of protein was performed, which determined that an active protein concentration of 1 μM was required for robust and reproducible signal after irradiation.

Assay protocol optimisation

The biochemistry and analysis components of the workflow were also optimised to increase assay throughput (Figure 3B). Automated acoustic dispensing was introduced for accurate plating of nanolitre volumes of competitor compounds. Irradiation time was optimised to 1 min, which afforded full photoactivation of probe **1** (Figure 1D). Higher throughput intact protein LCMS methods were developed (5.75 min/sample) by optimising solvent flow rates, gradients, and wash cycles. To improve the throughput and integrity of the data analysis component of the workflow, bespoke R scripts were written, which performed automated calculation of percentage labelling from deconvoluted intact protein mass spectra.

Single-shot screening of known BET inhibitors

To obtain a test set of compounds known to bind to BET domains, the ChEMBL database was queried for compounds that had annotated activity against the BET family. A subset of these compounds was selected based on availability, yielding 264 compounds (Supplementary Table S1). The compounds were screened against BD1 and BD2 simultaneously at a single concentration in duplicate following the optimised assay workflow (Figure 3B). Solutions of PAL probe **1** (5 μM) and BRD4 BD1 and BD2 (1 μM each) were added to the

Biochemical Journal (2023) **480** 1183–1197
https://doi.org/10.1042/BCJ20230129

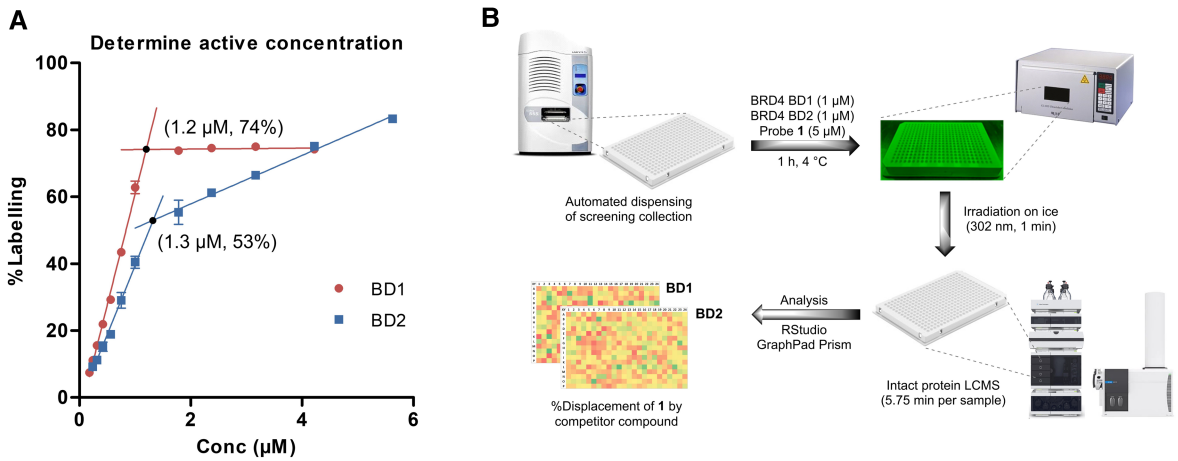

Figure 3. Determining the active concentration of protein and optimising the biochemical workflow.
(**A**) Experiment to determine the active concentrations of BRD4 BD1 and BD2. These values were used to accurately adjust protein active concentration to 1.0 μM in the assay. (**B**) Optimised PAL displacement assay workflow. Competitor compounds were acoustically dispensed into 384-well low-volume plates (150 nL). A solution of BRD4 BD1 and BD2 protein (1 μM) and **1** (5 μM) was added to each well. After 1 h equilibration on ice, the plates were irradiated (302 nm, 1 min) and sealed before being analysed directly by intact protein LCMS (5.75 min/sample). The BD1 and BD2 protein peaks were deconvoluted and this data was further analysed using RStudio and GraphPad Prism.

competitor compound (100 μM), and the plates were equilibrated on ice (1 h) and irradiated (1 min). The extent of photocrosslinking by probe **1** to both domains was then determined using intact protein LCMS (eqn 1). These values were normalised by subtraction of non-specific labelling and division by the maximum labelling observed (eqn 2). The resulting normalised labelling was converted to percentage displacement (eqn 3) and averaged over the two replicates (Supplementary Table S1) [23].

$$\%\,\text{Labelling} = \frac{\text{peak height for single labelled protein}}{(\text{peak height for unlabelled protein} + \text{single labelled protein})} \times 100 \quad (1)$$

$$\%\,\text{normalised labelling} = \frac{\%\ \text{labelling} - \text{A}}{\text{B} - \text{A}} \times 100 \quad (2)$$

A = lowest % labelling observed (most potent competitor)
B = highest % labelling observed (DMSO control)

$$\%\ \text{displacement} = 100 - \%\ \text{normalised labelling} \quad (3)$$

The data for BD1 was found to be more reproducible than for BD2, showing a tighter correlation between each replicate (R^2 of 0.95 and 0.78, respectively) (Figure 4A,B). The lower correlation between replicates for BD2 was attributed to the greater noise observed in the deconvoluted mass spectra (see Supplementary Figure S2). Comparison of displacement values for BD1 and BD2 revealed compounds that appeared to be either BD1 or BD2 selective (e.g. **F02** and **C01**, respectively), along with potent competitors at both domains (e.g. **A02**, **H01** and **K01**) (Figure 4C). From the 264 compounds screened, 42 compounds showed ≥60% displacement at either or both domains and were selected for screening in full-curve concentration-response format.

Full-curve concentration-response screening

The 42 competitor compounds selected from the preliminary single-shot screening were dispensed in an 8-point serial dilution (1 in 2) with a final concentration ranging from 100 μM to 0.78 μM. A DMSO control was included as the ninth data point. The compounds were screened in duplicate following the optimised assay workflow described in Figure 3B. To account for non-specific labelling, percentage total labelling was calculated

Biochemical Journal (2023) **480** 1183–1197
https://doi.org/10.1042/BCJ20230129

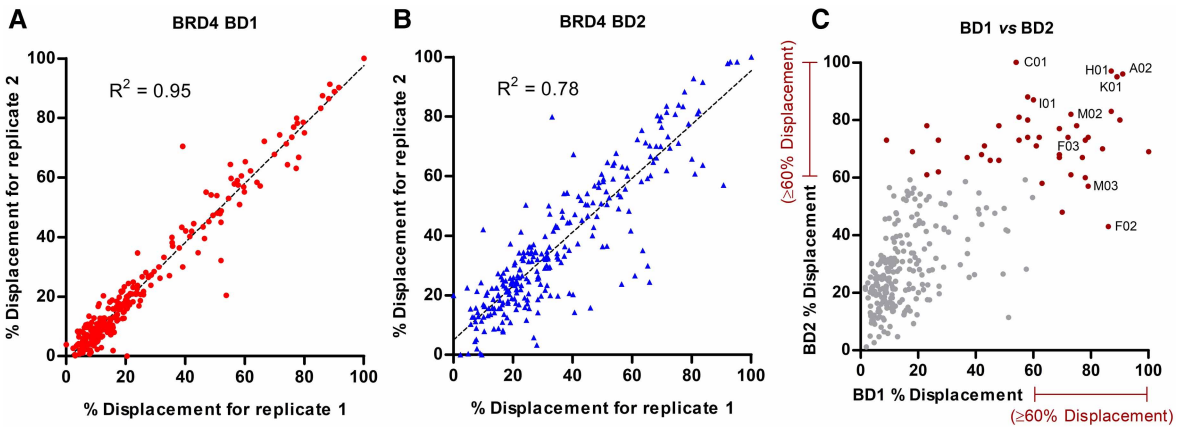

Figure 4. Robustness of single concentration screening.

(**A**) Replicate values of percentage displacement plotted for BRD4 BD1. (**B**) Replicate values of percentage displacement plotted for BRD4 BD2. (**C**) Mean values of percentage displacement plotted for both domains. Competitor compounds that displayed ≥60% displacement of PAL probe **1** (shown in red) were selected for screening in full-curve dose-response format.

using equation 4.

$$\%\,\text{labelling} = \frac{B + 2C}{A + B + 2C} \times 100 \tag{4}$$

where:

A = peak height for unlabelled protein
B = peak height for single labelled protein
C = peak height for double labelled protein

The data was fit using a four-parameter non-linear regression with a bottom constraint >0 (Figure 5 and Supplementary Figures S3–6). The majority of compounds exhibited similar potencies at both domains, consistent with the high sequence homology of the binding sites. Compound **C01** (i-BET295) showed selectivity for BD2, and compounds **F02** and **M03** (iBET-151) showed selectivity for BD1 [24,25]. **K01** (ABBV-075/Mivebresib) was highly potent against both BD1 and BD2 [26]. The dual-target ligands such as **H01** (dual HDAC/BET probe) and **M02** (BI-2356, dual PLK1/BRD4 inhibitor) gave well-defined curves and were equipotent at BD1 and BD2 [27,28].

Comparison to TR-FRET data

To compare the pIC_{50} values derived from the PAL assay to those obtained in an orthogonal biochemical assay, the set of 42 compounds was screened in BRD4 BD1 and BD2 TR-FRET assays [19]. The pIC_{50} values obtained from each assay gave a good correlation: R^2 of 0.75 and 0.71 for BD1 and BD2, respectively (Figure 6A), however, the PAL values were consistently lower than those obtained by TR-FRET. This off-set results from the high potency of the PAL ligand as compared with the peptide ligand used in the TR-FRET. Thus, PAL assay values were corrected using the Cheng–Prusoff equation with the Munson–Rodbard correction (eqn 5) [15]. The pIC_{50} values of PAL probe **1** in the TR-FRET assays (BD1/BD2 pIC_{50} = 7.8/7.3, respectively) were used as a surrogate for the K_d value at each domain. As 5 μM of PAL probe **1** (p*) was added to 1 μM of BD1 and BD2, the initial bound/free ratio of PAL probe (y_0) was entered as 2/3. The K_i values produced using equation 5 were transformed to pK_i values using equation 6.

$$K_i = \frac{IC_{50}}{1 + \dfrac{p^*(y_0 + 2)}{2K_d(y_0 + 1)} + y_0} + K_d\left(\frac{y_0}{y_0 + 2}\right) \tag{5}$$

where:

Biochemical Journal (2023) **480** 1183–1197
https://doi.org/10.1042/BCJ20230129

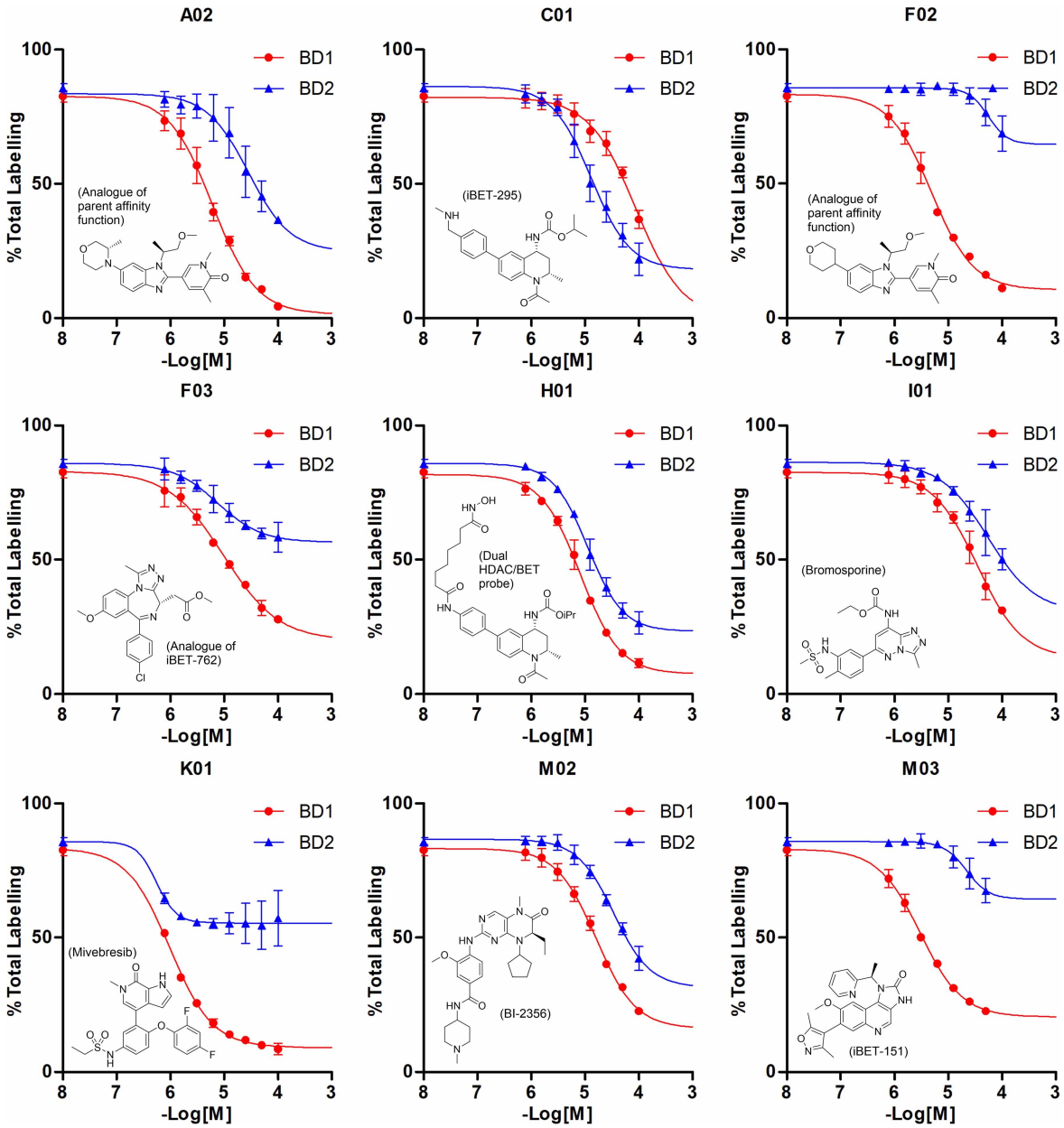

Figure 5. Concentration-response curves for selected bromodomain inhibitors.

Selected dose-response curves for known BET inhibitors as determined by PAL displacement assay. **F02** and **M03** showed selectivity for BRD4 BD1. **C01** showed selectivity for BRD4 BD2. The data was fitted with a four-parameter non-linear regression with a bottom constraint >0 (GraphPad Prism). The dose response curves for all 42 selected compounds are shown in Supplementary Figures S3–6.

IC_{50} = value obtained in the PAL displacement assay
p* = Initial concentration of PAL probe **1**
K_d = IC_{50} value for PAL probe obtained in the TR-FRET assays
y_0 = initial ratio of bound/free PAL probe

$$pK_i = -\log_{10} K_i \tag{6}$$

The derived pK_i values from the PAL assay showed good correlation with the TR-FRET data for both BD1 and

Biochemical Journal (2023) **480** 1183–1197
https://doi.org/10.1042/BCJ20230129

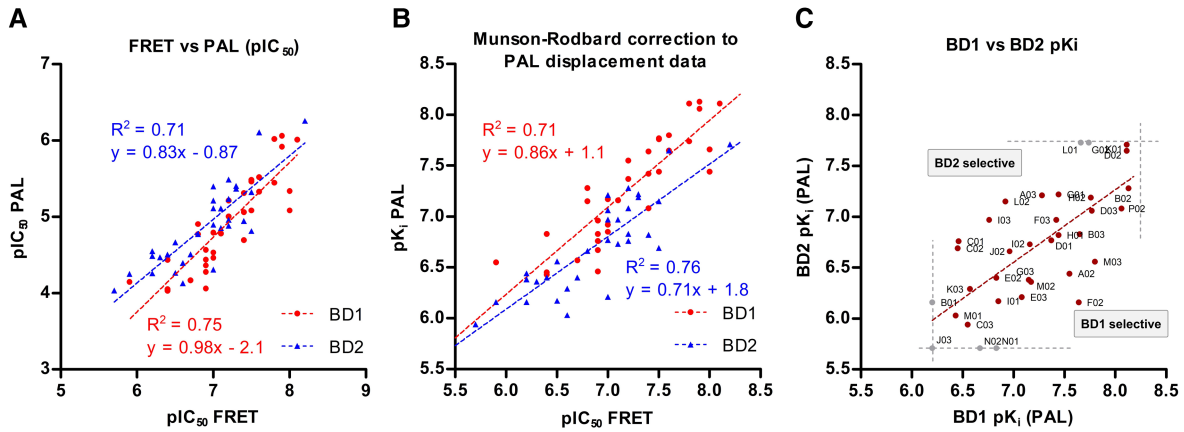

Figure 6. Comparison between photoaffinity displacement assay and TR-FRET values.

(**A**) Comparison of the pIC_{50} values obtained from the PAL displacement assay and from a TR-FRET biochemical assay. (**B**) Comparison of the derived pK_i values from the PAL displacement assay and the pIC_{50} values obtained from a TR-FRET assay for both domains. The pK_i values were obtained by transforming the IC_{50} values from the PAL displacement assay using the Munson–Rodbard correction to the Cheng–Prusoff equation. A good correlation was observed between the PAL displacement assay and the TR-FRET assay for both BD1 and BD2 domains ($R^2 = 0.71$ and 0.76). (**C**) Plotting the pK_i values for BD1 and BD2 derived from the IC_{50} values obtained in the PAL displacement assay. The lower and upper limits of the assay are shown by dashed grey lines.

BD2: $R^2 = 0.71$ and 0.76, respectively (Figure 6B and Table 1), supporting that the PAL displacement assay offers a viable biochemical screening method to inform on the relative affinities of competitor compounds to two target proteins simultaneously.

To explore the use of this assay as a means for determining the BD1/BD2 selectivity of compounds, the derived pK_i values for both domains were compared (Figure 6C). Compounds **C01**, **C02**, **I03** and **L02** were identified as BD2 selective (≤0.4-fold), which was consistent with the TR-FRET assays (see Table 1). **L01** and **G02** (iBET-295) were also identified as highly potent and selective BD2 ligands, which were above the upper limit of the PAL assay for BD2. Compounds **F02**, **A02**, **M03** (iBET-151), **M02**, **P02**, **B02**, **E03** were identified as BD1 selective ligands, which also agreed with the selectivity observed in the TR-FRET assays (Table 1). By benchmarking the PAL assay against orthogonal TR-FRET assays for BD1 and BD2, this study demonstrated that a dual-domain PAL displacement assay could be used to measure relative affinities and selectivity of competing ligands for both the BD1 and BD2 domains within the same experiment.

Discussion

This work reports the development and optimisation of a PAL displacement assay, capable of reporting affinities to multiple recombinant protein domains in tandem. By using a pan-BRD PAL probe **1** as a reporter compound, the relative affinities of BRD inhibitors were measured against BRD4 BD1 and BD2 simultaneously. PAL probe **1** was chosen as the assay reporter due to the high photocrosslinking yields observed with both target proteins, and for its rapid photoactivation rate (302 nm, ≤1 min), which minimised the required exposure of protein to damaging UV irradiation. The practical components of the assay platform were optimised to afford a simple and effective workflow in which compounds were dispensed in 384 well plates before addition of solutions of PAL probe **1** and protein. Plates were subsequently irradiated with UV light and then analysed by intact LCMS. Bespoke R scripts were written to perform automated data processing and calculation of photocrosslinking yields (Figure 3B). Remaining optimisation requirements of the assay include reduction in LCMS analysis time to improve throughput, and reduction in protein concentration requirements to improve the dynamic range. Faster sampling technologies such as Rapidfire MS (*ca.* 8 s per sample) or RapiFlex MALDI MS (*ca.* 0.3 s per sample) may be applicable to increase the throughput of the assay platform [34,35]. Later intact protein LCMS instruments that can obtain good protein signal-to-noise spectra with lower protein concentrations (e.g. Agilent ToF G6230B) than the instrument used in this work (Agilent ToF G6224A) would improve the dynamic range of the assay.

Biochemical Journal (2023) **480** 1183–1197
https://doi.org/10.1042/BCJ20230129

Table 1 TR-FRET, single-shot PAL displacement, and full-curve PAL displacement data for the 42 competitor compounds screened against BRD4 BD1 and BD2

Competitor compound	Compound details	BD1 TR-FRET (pIC_{50})	BD2 TR-FRET (pIC_{50})	% Disp. BD1 (single-shot)	% Disp. BD2 (single-shot)	BD1 PAL (full-curve) (pIC_{50})	BD2 PAL (full-curve) (pIC_{50})	BD1 PAL (full-curve) (pK_i)	BD2 PAL (full-curve) (pK_i)
A02	Analogue of PAL probe affinity function[29]	7.2	6.2	91	96	5.2	4.5	7.6	6.4
A03	Analogue of iBET-762[30]	6.8	7.0	42	68	4.9	5.4	7.3	7.2
B01	Analogue of iBET-762[30]	5.5	5.9	18	69	<3.8	4.3	<6.2	6.2
B02	Analogue of PAL probe affinity function[29]	7.9	7.2	100	69	6.1	5.5	8.1	7.3
B03	Analogue of PAL probe affinity function[29]	7.6	7.2	84	70	5.3	5	7.7	6.8
C01	iBET-295[27]	6.9	7.2	54	100	4.1	4.9	6.5	6.8
C02		6.4	7.5	23	78	4.1	4.8	6.5	6.7
C03	Dual HDAC/BET probe[27]	5.9	5.7	27	73	4.1	4	6.5	5.9
D01		7.2	7.0	75	78	5	4.9	7.4	6.8
D02	Analogue of PAL probe affinity function[29]	7.8	7.6	87	83	6	6.1	8.1	7.7
D03	Analogue of iBET-151[25]	7.5	7.0	78	73	5.5	5.2	7.8	7.1
E01	TG-101209 (Dual JAK2/BRD4 inhibitor)[31]	5.9	5.6	58	80	4.4	4.6	6.8	6.5
E02		6.9	6.7	69	68	4.4	4.5	6.8	6.4
E03		7.4	7.0	73	61	4.7	4.3	7.1	6.2
F02	Analogue of PAL probe affinity function[29]	7.4	6.2	86	43	5.3	4.3	7.6	6.2
F03	Analogue of iBET-762[30]	7.4	7.0	72	74	5.1	5.1	7.4	7.0
G01	Analogue of iBET-762[30]	7.5	7.3	63	58	5.1	5.4	7.4	7.2
G02	iBET-726[24]	7.8	8.2	90	80	5.4	>6.3	7.7	>7.7
G03	Analogue of iBET-151[25]	6.8	6.2	79	74	4.8	4.5	7.2	6.4
H01	Dual HDAC/BET probe[27]	8.0	7.4	87	97	5.1	4.9	7.4	6.8
H02	Analogue of iBET-151[25]	7.5	7.3	78	60	5.5	5.4	7.8	7.2
H03	Dual kinase/BRD4 inhibitor[28]	6.4	6.0	48	78	3.9	<3.8	6.3	<5.7
I01	Bromosporine[32]	7.0	6.5	60	87	4.5	4.3	6.9	6.2
I02		7.1	7.1	55	73	4.8	4.9	7.2	6.7
I03	Analogue of iBET-762[30]	6.9	7.1	62	74	4.4	5.1	6.8	7.0
J01		5.8	5.7	27	62	<3.8	4.8	<6.2	6.7
J02		6.9	6.8	69	67	4.6	4.8	7	6.7
J03		5.9	5.9	43	71	<3.8	<3.8	<6.2	<5.7
K01	ABBV-075/Mivebresib[26]	8.1	8.2	89	95	6	6.3	8.1	7.7
K02		5.3	6.4	9	73	NA	4.5	NA	6.4
K03		6.7	6.6	48	66	4.2	4.4	6.6	6.3
L01	Analogue of iBET-726[24]	8.0	8.5	69	77	5.3	>6.3	7.7	7.7
L02	Analogue of iBET-762[30]	7.0	7.5	61	71	4.5	5.3	6.9	7.1
M01		6.4	6.6	29	42	4	4.1	6.4	6.0
M02	BI-2356 (Dual PLK1/BRD4 inhibitor)[28]	7.0	6.3	73	82	4.8	4.5	7.2	6.4
M03	iBET-151[25]	7.6	6.5	79	57	5.5	4.7	7.8	6.6
N01	Analogue of iBET-151[25]	6.4	5.8	70	48	4.4	<3.8	6.8	<5.7
N02	Analogue of iBET-762[30]	6.9	6.9	58	74	4.3	<3.8	6.7	<5.7
O01	Benzo[cd]indol-2(1H)-one BET inhibitor[33]	5.6	4.5	23	61	4.3	<3.8	6.7	<5.7
O02		NA	NA	45	66	3.9	3.9	6.3	5.8
P01		4.8	4.8	37	67	<3.8	3.9	<6.2	5.8
P02	Analogue of iBET-151[25]	7.9	7.2	77	67	5.9	5.2	8.1	7.1

pIC_{50} and pK_i values coloured red, yellow, green for low, medium, high values, respectively.

A set of 264 compounds with reported BET activity in the CHEMBL database were selected for profiling against BD1 and BD2 in the assay. Initially, compounds were screened at a single high concentration (100 μM) in duplicate, which identified 42 compounds that showed ≥60% inhibition of labelling at either domain. These compounds were structurally diverse and included a range of well-known BET inhibitors such as iBET-295 (**C01**), TG 101209 (**E01**), iBET-726 (**G02**), bromosporine (**I01**), Mivebresib (**K01**), BI-2356 (**M02**) and

Biochemical Journal (2023) **480** 1183–1197
https://doi.org/10.1042/BCJ20230129

iBET-151 (**M03**). The 42 hit compounds were followed up in a 9-point concentration-response to obtain pIC_{50} values against both BD1 and BD2. These values were transformed using the Cheng–Prusoff equation to provide pK_i values, which showed excellent correlation with values determined by TR-FRET. The pK_i values were subsequently used to determine BD1/BD2 selectivity, which crucially agreed with the selectivity observed by TR-FRET, supporting the validity of the platform in selectivity profiling. It is anticipated that the assay could be further developed to include additional protein domains per sample to deliver richer information without extending assay time. For example, BET isoform selectivity could be measured for all N- and C-terminal domains of BRD2, BRD3, BRD4 and BRDT in tandem. One limitation of this approach is that only binding of the competitor compound to the same specific site as the PAL probe can be measured. In the majority of cases, measuring this specific binding to a known site would be desired. However, allosteric binding events of competitor compounds that induce no change to the binding affinity of the PAL probe to the protein will not be observed.

Generation of reporter ligands for this PAL-based assay platform has become more synthetically feasible, as multiple recent efforts have demonstrated PAL probes can be successfully accessed from a given parent affinity function [13,14,36–39]. Thus, the platform could be employed where selectivity over related off-targets is crucial. For example, a pan-JAK PAL probe could be used to screen against the family (JAK1, JAK2, JAK3 and TYK2) to aid identification of isoform selective compounds. JAK1 selective inhibitors have been marketed for the treatment of rheumatoid arthritis, e.g. Upadacitinib [40]. Alternatively, in cases where polypharmacology is desired, multiple on-targets could be assayed simultaneously using this approach. For example, Watts et al. [41] improved the selectivity profile of the known dual BRD4/ALK inhibitor BI-2536, by developing inhibitors with maintained on-target BRD4/ALK activity, but reduced off-target PLK-1 activity. A variety of assay techniques were used that all required dedicated assay development and unique technologies, while a PAL analogue of BI-2356 might enable measurement of potencies against all three protein targets at once.

Methods

Synthetic chemistry

PAL probes **1** to **15** were synthesised as previously described [14]. All BET inhibitors were available within the GSK compound collection.

Recombinant protein

BRD4 BD1 and BRD4 BD2 were prepared as previously described [14]. Briefly:

BRD4 BD1 (44–168) was obtained from GenScript:

6H-tev-BRD4 (44–168) was expressed in *E. coli* and purified by Ni-affinity chromatography (HisTRAP HP Affinity Column, GE Healthcare 17-5248-02). TEV cleavage and size-exclusion chromatography (Superdex 75pg SEC column) was performed to obtain BRD4 BD1 (44–168).

6H-tev-Brd4 (333–460):

6H-tev-Brd4 (333–460) was expressed in *E. coli* and purified by Ni-affinity chromatography (HisTRAP HP column, GE Healthcare 17-5248-02) followed by size-exclusion chromatography (Superdex 75pg SEC column).

Intact protein LCMS analysis

Samples were injected using an Agilent 1200 series AutoSampler (Model No. G1367B) with sample temperature maintained at 10°C. Chromatography was performed on an Agilent PLRP S reverse phase column (1000 Å, 5 μm × 50 mm × 1.0 mm, PL1312–1502) at 70°C and using an Agilent 1200 series binary pump system (Model No. G1312B) with 0.2% formic acid in water (Solvent A) and 0.2% formic acid in acetonitrile (Solvent B) following the gradient described in Table 2. Detection was performed using an Agilent ToF mass spectrometer (Model No. G6224A) with dual ESI source with a scan rate of 1.03 s in positive mode. Analysis was performed using Agilent MassHunter Qualitative Analysis Software (Version B.06.00).

Software details

The specific versions of software used for data collection and analysis can be found below in Table 3.

Table 2 Solvent gradient for intact protein LCMS method

Time (min)	Flow rate (ml min^{-1})	Solvent A (%)	Solvent B (%)
0.00	0.5	80	20
0.50	0.5	80	20
0.51	0.5	60	40
2.50	0.5	20	80
2.51	0.5	0	100
3.60	0.5	0	100
3.61	0.5	80	20
3.80	1.2	80	20
4.45	1.2	80	20
4.46	0.5	80	20

BRD4 BD1 and BD2 TR-FRET assays

BET proteins were produced using published protocols [42]. The TR-FRET assays for both BD1 and BD2 domains were performed following the published protocols [19].

Percentage labelling of 15 probes (1–15) to BD1 and BD2 after irradiation (302 nm, 10 min)

Each PAL probe (0.5 mM in DMSO, 150 nL, FAC = 5 μM) was transferred to four wells of a Greiner low volume 384-well plate using a Labcyte 555 Echo acoustic dispenser. The plate was placed on ice and a solution of BRD4 BD1 (1 μM in PBS, 15 μl) was added to the first two wells and a solution of BRD4 BD1 (1 μM in PBS, 15 μl) was added to the second two wells. The plate was sealed and allowed to equilibrate on ice for 1 h. then centrifuged (1000 rpm, 1 min, rt). The seal was removed, and the plate was irradiated on ice (302 nm, 10 min). The UV lamp was warmed for 2 min prior to sample irradiation. The plate was sealed and centrifuged (1000 rpm, 1 min, rt) before being sampled directly for intact protein LCMS analysis. The total ion chromatograms (TIC) were extracted (region containing protein) and the summed scans were deconvoluted using a maximum entropy algorithm between 700–2200 Da with an expected mass range of 14 000–20 000 Da for both BD1 and BD2. The peak areas for unmodified protein and for single, double, and triple labelled protein were recorded for each duplicate. Percentage single labelling and excess labelling were calculated using equation 7 and equation 8, respectively, and then averaged over two replicates. These data were plotted on a stacked and grouped column plot (Figure 2B). Error bars show ±1 standard deviation.

$$\%\ \text{single labelling} = \frac{\text{Peak area for single labelled protein}}{(\text{Sum of Peak areas for all recorded peaks})} \times 100 \tag{7}$$

$$\%\ \text{excess labelling} = \frac{\text{Sum of peak areas for excess labelling}}{(\text{Sum of Peak areas for all recorded peaks})} \times 100 \tag{8}$$

Table 3 Software packages and versions used for analysis

Software	Use
GraphPad Prism for Windows (Version 5.04, 2010)	Plotting binding curves and dose-response curves
Agilent MassHunter Qualitative Analysis Software (Version B.06.00)	Analysing intact protein LCMS data
Rstudio (Version 0.98.978)	Interpreting intact protein LCMS deconvoluted spectra
R 3.5.1	Version of R language used for interpreting intact protein LCMS spectra in RStudio IDE

Biochemical Journal (2023) **480** 1183–1197
https://doi.org/10.1042/BCJ20230129

Photocrosslinking time course for probe 2.45 with BD1 and BD2

Probe **1** (0.5 mM in DMSO, 60 μl, FAC = 5 μM) was added to a stock solution of BRD4 BD1 and BD2 (1 μM each, 6 ml in PBS) on ice. The mixture was equilibrated on ice for 30 min. An amount of 15 μl was transferred to row A, columns 1 and 2 (duplicates) of an irradiation plate (Greiner 384-well low volume, 784075). The plate was irradiated (302 nm) on ice for the time given in Table 4.

The plate was sealed and sampled directly for intact protein LCMS analysis. The TIC were extracted (region containing protein) and the summed scans were deconvoluted using a maximum entropy algorithm between 750–2200 Da with an expected mass range of 14 000–21 000 Da. A .csv file of the deconvoluted spectra (Counts *vs* Mass (Da)) was exported and interpreted using RStudio (Version 0.98.978, R 3.5.1). The peak heights for unmodified, single labelled and double labelled protein were used to calculate percentage single labelling using equation 7 for BD1 and BD2 for each replicate. These data were exported as a .csv file and interpreted in Excel to obtain average percentage labelling and standard deviation for the duplicates. These data were transferred to GraphPad Prism and plotted on an XY scatter plot *vs* irradiation time and fitted with a non-linear regression (one-phase decay). Error bars show ±1 standard deviation.

Experiments to determine the active concentration of BD1 and BD2

A 19-point serial dilution (0.75×) of **1** was prepared in a Greiner 384 square well plate from a stock of 1 mM in DMSO (1 mM to 0.0056 mM over 19 points, with DMSO control as point 20). An amount of 150 nL of each well was transferred to two daughter Greiner 384 low-volume plates using a Labcyte Echo 555 acoustic dispenser in triplicate (Rows A–C, columns 1–20). The daughter plates were placed on ice and a solution of BRD4 BD1 (estimated from stock to be 1 μM, 15 μl) was added to each well of the first plate, and BRD4 BD2 (estimated from stock to be 2 μM, 15 μl) was added to each well of the second plate. The plates were sealed and centrifuged (1000 rpm, 1 min, rt) and equilibrated on ice for 20 min. The seals were removed, and the plates were irradiated (302 nm, 0.6 min) on ice. The UV lamp was warmed for 2 min prior to sample irradiation. The plate was sealed and sampled directly for intact protein LCMS analysis. The TIC were extracted (regions containing protein) and the summed scans were deconvoluted using a maximum entropy algorithm between 800–2200 Da for BD1 and 750–2200 Da for BD1 with an expected mass range of 14 000–21 000 Da for both proteins. A csv file of the deconvoluted spectra (Counts *vs* Mass (Da)) was exported and interpreted using RStudio (Version 0.98.978, R 3.5.1). The peak heights for unmodified, single labelled, double labelled and triple labelled protein were used to calculate percentage labelling using equation 7 for BD1 and BD2 for each replicate. Percentage total labelling was calculated as the sum of percentage single, double and triple labelling. The average percentage total labelling and standard deviation for the triplicates for both proteins were transferred to GraphPad Prism and plotted on an XY scatter plot *vs* concentration of **1**. The linear portions of each plot were re-plotted and fitted with linear regression to obtain the active protein concentration. Error bars show ±1 standard deviation.

Single concentration PAL displacement assay with the ChEMBL set of competitor compounds

ChEMBL set of competitor compounds (10 mM in DMSO, 150 nL, FAC = 100 μM) were transferred to two duplicate daughter Greiner low-volume 384 well plates (one compound per well). A mixture of BRD4 BD1 (1 μM), BRD4 BD2 (1 μM) and **1** (5 μM) in PBS (0.1% DMSO) was prepared and 15 μl was added to each

Table 4 Irradiation times for the photocrosslinking time course of PAL probe 1

Row:	Irradiation time for each row (min):	Total irradiation time for each row (min):
A	1.0	2.0
B	0.5	1.0
C	0.2	0.5
D	0.2	0.3
E	0.1	0.1
F	0.0	0.0

sample well on ice (final percentage of DMSO = 1.1%). The plates were sealed and centrifuged (1000 rpm, 1 min, rt) and equilibrated on ice for 1 h. The seals were removed, and the plates were irradiated on ice (302 nm, 0.6 min). The UV lamp was warmed for 2 min prior to sample irradiation. The plates were sealed and sampled directly for intact protein LCMS analysis. The TIC were extracted (regions containing protein) and the summed scans were deconvoluted using a maximum entropy algorithm between 750–2200 Da with an expected mass range of 14 000–21 000 Da for both proteins. A .csv file of the deconvoluted spectra (Counts *vs* Mass (Da)) was exported and interpreted using RStudio (Version 0.98.978, R 3.5.1). The peak heights for unmodified and single labelled protein were used to calculate percentage labelling using equation 1. The percentage normalised labelling and percentage displacement were calculated for each compound following equation 2 and equation 3, respectively. The experiment was performed in duplicate. The percentage displacement from both replicates were plotted against each other for both BD1 and BD2 in XY scatter plots using Graphpad Prism (Figure 4A,B). The average percentage displacement for BD1 and BD2 over the two replicates given in Supplementary Table S1 were plotted against each other in an XY scatter plot using GraphPad Prism (Figure 4C). Compounds that showed and average percentage displacement of ≥60% to either BD1 or BD2 were chosen for follow-up dose response experiments.

Full-curve dose-response PAL displacement assay with the compounds selected from single-shot screening

An 8-point, 1-in-2 serial dilution of the 42 competitor compounds chosen from the preliminary single-shot PAL screen (+DMSO only treated as a 45th compound) was prepared in an Echo Qualified 384-Well Low Dead Volume Microplate (384LDV-Black). This plate was then transferred to two duplicate daughter Greiner low-volume 384 well plates (150 nL per well) using a Labcyte Echo555 acoustic dispenser. A mixture of BRD4 BD1 (1 μM), BRD4 BD2 (1 μM) and **1** (5 μM) in PBS (0.1% DMSO) was prepared and 15 μl was added to each sample well of both daughter plates on ice (final concentration of DMSO = 1.1%). The plates were sealed and centrifuged (1000 rpm, 1 min, rt) and equilibrated on ice for 1 h. The seals were removed, and the plates were irradiated on ice (302 nm, 1.0 min). The UV lamp was warmed for 2 min prior to sample irradiation. The plates were sealed and sampled directly for intact protein LCMS analysis. The TIC were extracted (region containing protein) and the summed scans were deconvoluted using a maximum entropy algorithm between 750–2200 Da with an expected mass range of 14 000–21 000 Da for both proteins. A csv file of the deconvoluted spectra (Counts *vs* Mass (Da)) was exported and interpreted using RStudio (Version 0.98.978, R 3.5.1). The peak heights for unmodified, single labelled and double labelled protein were used to calculate percentage total labelling using equation 4.

The values for total percentage labelling were averaged over the two replicates and plotted against the $-\log_{10}$[competitor]. These data were fit with a 'log(agonist) vs. response – Variable slope (four parameters)' nonlinear regression with no top constraint, and a bottom constraint of greater than zero using Graphpad Prism. The average percentage total labelling for the DMSO controls was included as the ninth data point for each compound. These plots for the 42 compounds (+DMSO) are shown in Supplementary Figures S3–6. The IC_{50} values obtained from each curve were transformed to pIC_{50} values using $IC_{50} = -\log_{10}(IC_{50})$. These values were plotted against the pIC_{50} values obtained for the 42 compounds in BD1 and BD2 TR-FRET assays (Figure 6A). The IC_{50} values obtained from the PAL displacement assay were transformed to apparent K_i values following the Munson–Rodbard correction to the Cheng–Prusoff equation (eqn 5) [15]

The apparent K_i values were then transformed to pK_i values using equation 6. These pK_i values were plotted against the pIC_{50} values obtained in BD1 and BD2 TR-FRET assays (Figure 4B). The pK_i values for BD1 and BD2 were plotted against each other on an XY scatter plot (Figure 4C). The TR-FRET data, PAL single-shot percentage displacement data, PAL pIC_{50} data and the transformed pK_i data for both BD1 and BD2 domains for the 42 compounds screened is given in Table 1.

Data Availability

The authors declare that all data supporting the findings and conclusions of this study are available within the article or Supplementary Data File.

Competing Interests

The authors declare that there are no competing interests associated with the manuscript.

Biochemical Journal (2023) **480** 1183–1197
https://doi.org/10.1042/BCJ20230129

Funding

We thank the GlaxoSmithKline/University of Strathclyde Collaborative PhD. programme for funding this work. We thank the EPSRC for funding via Prosperity Partnership EP/S035990/1, along with a Postgraduate and Early Career Researcher Exchanges (PECRE) grant from the Scottish Funding Council (H17014).

CRediT Author Contribution

Jacob Bush: Conceptualization, Supervision, Writing — review and editing. **David Fallon:** Conceptualization, Data curation, Formal analysis, Investigation, Writing — original draft, Writing — review and editing. **Alex Phillipou:** Data curation, Formal analysis, Investigation, Writing — review and editing. **Christopher J. Schofield:** Conceptualization, Writing — review and editing. **David House:** Writing — review and editing. **Nicholas Tomkinson:** Conceptualization, Supervision, Writing — review and editing.

Acknowledgements

We would like to thank Daniel Thomas and Jon Hutchinson for their useful insights into biochemical assay development.

Abbreviations

BD, bromodomain; BET, bromodomain and extra-terminal domain; FP, fluorescence polarisation; PAL, photoaffinity labelling; TIC, total ion chromatograms; TR-FRET, time-resolved fluorescence resonance energy transfer.

References

1 Croston, G.E. (2017) The utility of target-based discovery. *Expert Opin. Drug Discov.* **12**, 427–429 https://doi.org/10.1080/17460441.2017.1308351
2 Eder, J., Sedrani, R. and Wiesmann, C. (2014) The discovery of first-in-class drugs: origins and evolution. *Nat. Rev. Drug Discov.* **13**, 577–587 https://doi.org/10.1038/nrd4336
3 Genick, C.C. and Wright, S.K. (2017) Biophysics: for HTS hit validation, chemical lead optimization, and beyond. *Expert Opin. Drug Discov.* **12**, 897–907 https://doi.org/10.1080/17460441.2017.1349096
4 Renaud, J.P., Chung, C.W., Danielson, U.H., Egner, U., Hennig, M., Hubbard, R.E. et al. (2016) Biophysics in drug discovery: impact, challenges and opportunities. *Nat. Rev. Drug Discov.* **15**, 679–698 https://doi.org/10.1038/nrd.2016.123
5 Mayr, L.M. and Bojanic, D. (2009) Novel trends in high-throughput screening. *Curr. Opin. Pharmacol.* **9**, 580–588 https://doi.org/10.1016/j.coph.2009.08.004
6 Fang, X., Zheng, Y., Duan, Y., Liu, Y. and Zhong, W. (2019) Recent advances in design of fluorescence-based assays for high-throughput screening. *Anal. Chem.* **91**, 482–504 https://doi.org/10.1021/acs.analchem.8b05303
7 Rectenwald, J.M., Hardy, P.B., Norris-Drouin, J.L., Cholensky, S.H., James, L.I., Frye, S.V. et al. (2019) A general TR-FRET assay platform for high-throughput screening and characterizing inhibitors of methyl-lysine reader proteins. *SLAS Discov.* **24**, 693–700 https://doi.org/10.1177/2472555219844569
8 Yasgar, A., Jadhav, A., Simeonov, A. and Coussens, N.P. (2016) AlphaScreen-Based Assays: Ultra-High-Throughput Screening for Small-Molecule Inhibitors of Challenging Enzymes and Protein-Protein Interactions. In *High Throughput Screening: Methods and Protocols* (Janzen, W.P., ed.), pp. 77–98, Springer New York, New York, NY
9 Hall, M.D., Yasgar, A., Peryea, T., Braisted, J.C., Jadhav, A., Simeonov, A. et al. (2016) Fluorescence polarization assays in high-throughput screening and drug discovery: a review. *Methods Appl. Fluoresc.* **4**, 022001 https://doi.org/10.1088/2050-6120/4/2/022001
10 Janzen, W.P. (2014) Screening technologies for small molecule discovery: the state of the art. *Cell Chem. Biol.* **21**, 1162–1170 https://doi.org/10.1016/j.chembiol.2014.07.015
11 Burton, N.R., Kim, P. and Backus, K.M. (2021) Photoaffinity labelling strategies for mapping the small molecule-protein interactome. *Org. Biomol. Chem.* **19**, 7792–7809 https://doi.org/10.1039/d1ob01353j
12 Grant, E.K., Fallon, D.J., Hann, M.M., Fantom, K.G.M., Quinn, C., Zappacosta, F. et al. (2020) A photoaffinity-based fragment-screening platform for efficient identification of protein ligands. *Angew. Chem. Int. Ed. Engl.* **59**, 21096–21105 https://doi.org/10.1002/anie.202008361
13 Thomas, R.P., Heap, R.E., Zappacosta, F., Grant, E.K., Pogany, P., Besley, S. et al. (2021) A direct-to-biology high-throughput chemistry approach to reactive fragment screening. *Chem. Sci.* **12**, 12098–12106 https://doi.org/10.1039/d1sc03551g
14 Fallon, D.J., Lehmann, S., Chung, C.W., Phillipou, A., Eberl, C., Fantom, K.G.M. et al. (2021) One-step synthesis of photoaffinity probes for live-cell MS-based proteomics. *Chemistry* **27**, 17880–17888 https://doi.org/10.1002/chem.202102036
15 Munson, P.J. and Rodbard, D. (1988) An exact correction to the "Cheng-Prusoff" correction. *J. Recept. Res.* **8**, 533–546 https://doi.org/10.3109/10799898809049010
16 Grant, E.K., Fallon, D.J., Eberl, H.C., Fantom, K.G.M., Zappacosta, F., Messenger, C. et al. (2019) A photoaffinity displacement assay and probes to study the cyclin-dependent kinase family. *Angew. Chem. Int. Ed. Engl.* **58**, 17322–17327 https://doi.org/10.1002/anie.201906321
17 Gilan, O., Rioja, I., Knezevic, K., Bell, M.J., Yeung, M.M., Harker, N.R. et al. (2020) Selective targeting of BD1 and BD2 of the BET proteins in cancer and immunoinflammation. *Science* **368**, 387–394 https://doi.org/10.1126/science.aaz8455
18 Shorstova, T., Foulkes, W.D. and Witcher, M. (2021) Achieving clinical success with BET inhibitors as anti-cancer agents. *Br. J. Cancer* **124**, 1478–1490 https://doi.org/10.1038/s41416-021-01321-0

19 Law, R.P., Atkinson, S.J., Bamborough, P., Chung, C.W., Demont, E.H., Gordon, L.J. et al. (2018) Discovery of tetrahydroquinoxalines as bromodomain and extra-terminal domain (BET) inhibitors with selectivity for the second bromodomain. *J. Med. Chem.* **61**, 4317–4334 https://doi.org/10.1021/acs.jmedchem.7b01666
20 Faivre, E.J., McDaniel, K.F., Albert, D.H., Mantena, S.R., Plotnik, J.P., Wilcox, D. et al. (2020) Selective inhibition of the BD2 bromodomain of BET proteins in prostate cancer. *Nature* **578**, 306–310 https://doi.org/10.1038/s41586-020-1930-8
21 Lea, W.A. and Simeonov, A. (2011) Fluorescence polarization assays in small molecule screening. *Expert Opin. Drug Discov.* **6**, 17–32 https://doi.org/10.1517/17460441.2011.537322
22 Zeder-Lutz, G., Benito, A. and Van Regenmortel, M.H.V. (1999) Active concentration measurements of recombinant biomolecules using biosensor technology. *J. Mol. Recognit.* **12**, 300–309 https://doi.org/10.1002/(sici)1099-1352(199909/10)12:5<300::Aid-jmr467>3.0.Co;2-n
23 Campbell, R.M., Dymshitz, J., Eastwood, B.J., Emkey, R., Greenen, D.P., Heerding, J.M. et al. (2004) *Data Standardization for Results Management*, Eli Lilly & Company and the National Center for Advancing Translational Sciences, Bethesda, MD
24 Gosmini, R., Nguyen, V.L., Toum, J., Simon, C., Brusq, J.M., Krysa, G. et al. (2014) The discovery of I-BET726 (GSK1324726A), a potent tetrahydroquinoline ApoA1 up-regulator and selective BET bromodomain inhibitor. *J. Med. Chem.* **57**, 8111–8131 https://doi.org/10.1021/jm5010539
25 Mirguet, O., Lamotte, Y., Donche, F., Toum, J., Gellibert, F., Bouillot, A. et al. (2012) From ApoA1 upregulation to BET family bromodomain inhibition: discovery of I-BET151. *Bioorg. Med. Chem. Lett.* **22**, 2963–2967 https://doi.org/10.1016/j.bmcl.2012.01.125
26 Wang, L., Pratt, J.K., Soltwedel, T., Sheppard, G.S., Fidanze, S.D., Liu, D. et al. (2017) Fragment-based, structure-enabled discovery of novel pyridones and pyridone macrocycles as potent bromodomain and extra-terminal domain (BET) family bromodomain inhibitors. *J. Med. Chem.* **60**, 3828–3850 https://doi.org/10.1021/acs.jmedchem.7b00017
27 Atkinson, S.J., Soden, P.E., Angell, D.C., Bantscheff, M., Chung, C.-W., Giblin, K.A. et al. (2014) The structure based design of dual HDAC/BET inhibitors as novel epigenetic probes. *Medchemcomm* **5**, 342–351 https://doi.org/10.1039/c3md00285c
28 Karim, R.M., Bikowitz, M.J., Chan, A., Zhu, J.Y., Grassie, D., Becker, A. et al. (2021) Differential BET bromodomain inhibition by dihydropteridinone and pyrimidodiazepinone kinase inhibitors. *J. Med. Chem.* **64**, 15772–15786 https://doi.org/10.1021/acs.jmedchem.1c01096
29 Wellaway, C.R., Amans, D., Bamborough, P., Barnett, H., Bit, R.A., Brown, J.A. et al. (2020) Discovery of a bromodomain and extraterminal inhibitor with a low predicted human dose through synergistic use of encoded library technology and fragment screening. *J. Med. Chem.* **63**, 714–746 https://doi.org/10.1021/acs.jmedchem.9b01670
30 Mirguet, O., Gosmini, R., Toum, J., Clement, C.A., Barnathan, M., Brusq, J.M. et al. (2013) Discovery of epigenetic regulator I-BET762: lead optimization to afford a clinical candidate inhibitor of the BET bromodomains. *J. Med. Chem.* **56**, 7501–7515 https://doi.org/10.1021/jm401088k
31 Ember, S.W., Zhu, J.Y., Olesen, S.H., Martin, M.P., Becker, A., Berndt, N. et al. (2014) Acetyl-lysine binding site of bromodomain-containing protein 4 (BRD4) interacts with diverse kinase inhibitors. *ACS Chem. Biol.* **9**, 1160–1171 https://doi.org/10.1021/cb500072z
32 Picaud, S., Leonards, K., Lambert, J.P., Dovey, O., Wells, C., Fedorov, O. et al. (2016) Promiscuous targeting of bromodomains by bromosporine identifies BET proteins as master regulators of primary transcription response in leukemia. *Sci. Adv.* **2**, e1600760 https://doi.org/10.1126/sciadv.1600760
33 Xue, X., Zhang, Y., Liu, Z., Song, M., Xing, Y., Xiang, Q. et al. (2016) Discovery of benzo[cd]indol-2(1H)-ones as potent and specific BET bromodomain inhibitors: structure-based virtual screening, optimization, and biological evaluation. *J. Med. Chem.* **59**, 1565–1579 https://doi.org/10.1021/acs.jmedchem.5b01511
34 Leveridge, M., Buxton, R., Argyrou, A., Francis, P., Leavens, B., West, A. et al. (2014) Demonstrating enhanced throughput of RapidFire mass spectrometry through multiplexing using the JmjD2d demethylase as a model system. *J. Biomol. Screen.* **19**, 278–286 https://doi.org/10.1177/1087057113496276
35 De Cesare, V., Johnson, C., Barlow, V., Hastie, J., Knebel, A. and Trost, M. (2018) The MALDI-TOF E2/E3 ligase assay as universal tool for drug discovery in the ubiquitin pathway. *Cell Chem. Biol.* **25**, 1117–1127.e1114 https://doi.org/10.1016/j.chembiol.2018.06.004
36 Ge, J., Cheng, X., Tan, L.P. and Yao, S.Q. (2012) Ugi reaction-assisted rapid assembly of affinity-based probes against potential protein tyrosine phosphatases. *Chem. Comm.* **48**, 4453–4455 https://doi.org/10.1039/c2cc31294h
37 Kambe, T., Correia, B.E., Niphakis, M.J. and Cravatt, B.F. (2014) Mapping the protein interaction landscape for fully functionalized small-molecule probes in human cells. *J. Am. Chem. Soc.* **136**, 10777–10782 https://doi.org/10.1021/ja505517t
38 Hill, J.R. and Robertson, A.A.B. (2018) Fishing for drug targets: a focus on diazirine photoaffinity probe synthesis. *J. Med. Chem.* **61**, 6945–6963 https://doi.org/10.1021/acs.jmedchem.7b01561
39 Bush, J.T., Walport, L.J., McGouran, J.F., Leung, I.K.H., Berridge, G., van Berkel, S.S. et al. (2013) The Ugi four-component reaction enables expedient synthesis and comparison of photoaffinity probes. *Chem. Sci.* **4**, 4115–4120 https://doi.org/10.1039/c3sc51708j
40 Cohen, S.B., van Vollenhoven, R.F., Winthrop, K.L., Zerbini, C.A.F., Tanaka, Y., Bessette, L. et al. (2021) Safety profile of upadacitinib in rheumatoid arthritis: integrated analysis from the SELECT phase III clinical programme. *Ann. Rheum. Dis.* **80**, 304–311 https://doi.org/10.1136/annrheumdis-2020-218510
41 Watts, E., Heidenreich, D., Tucker, E., Raab, M., Strebhardt, K., Chesler, L. et al. (2019) Designing dual inhibitors of anaplastic lymphoma kinase (ALK) and bromodomain-4 (BRD4) by tuning kinase selectivity. *J. Med. Chem.* **62**, 2618–2637 https://doi.org/10.1021/acs.jmedchem.8b01947
42 Chung, C.W., Coste, H., White, J.H., Mirguet, O., Wilde, J., Gosmini, R.L. et al. (2011) Discovery and characterization of small molecule inhibitors of the BET family bromodomains. *J. Med. Chem.* **54**, 3827–3838 https://doi.org/10.1021/jm200108t